Published in final edited form as:
J Magn Reson Imaging. 2010 September ; 32(3): 654–662. doi:10.1002/jmri.22258.

Post-Processing Correction of the Endorectal Coil Reception Effects in MR Spectroscopic Imaging of the Prostate

Susan M. Noworolski, PhD[1,2,*], **Galen D. Reed, BS**[1,2], **John Kurhanewicz, PhD**[1,2], and **Daniel B. Vigneron, PhD**[1,2]

[1] Department of Radiology and Biomedical Imaging, The University of California, San Francisco, California, USA

[2] The Graduate Group in Bioengineering, The University of California, San Francisco and Berkeley, California, USA

Abstract

Purpose—To develop and validate a post-processing correction algorithm to remove the effect of the inhomogeneous reception profile of the endorectal coil on MR spectroscopic imaging (MRSI) data.

Materials and Methods—A post-processing algorithm to correct for the endorectal coil reception effects on MRSI data was developed based upon theoretical modeling of the endorectal coil reception profile and of the spatial saturation pulse profiles. This algorithm was evaluated on three-dimensional (3D) MRSI data acquired at 3T from a uniform phantom and from 18 patients with known or suspected prostate cancer.

Results—For the phantom data, the coefficient of variation of metabolite peak areas decreased 16% to 46% and the peak area distributions became more Gaussian with correction, as demonstrated by higher Q-Q plot linear correlations ($R^2 = 0.98 \pm 0.007$ vs. $R^2 = 0.89 \pm 0.066$). Across the 18 patients, the mean coefficient of variation for suppressed water decreased significantly, from 0.95 ± 0.18, to 0.66 ± 0.11, ($P < 10^{-6}$, paired *t*-test) and the linear correlations of the Q-Q plots for the suppressed water increased from $R^2 = 0.91$ to $R^2 = 0.95$ ($P = 0.0083$, paired *t*-test) with correction.

Conclusion—An algorithm for reducing the effect of the inhomogeneous reception profile in endorectal coil acquired 3D MRSI prostate data was demonstrated, illustrating increased homogeneity and more Gaussian peak area distributions.

Keywords

endorectal coil; prostate; magnetic resonance spectroscopic imaging; correction; reception profile

Prostate cancer strikes one in six American males. It is the second leading cause of cancer death in men (1). The decision as to how best to manage individual prostate cancer patients is a difficult dilemma. Prostate cancer is one of the only cancers that can grow so slowly that it will never threaten some patients. However, if in others the cancer escapes the prostate, it becomes incurable. A noninvasive method that could identify, localize and characterize prostate cancers in terms of their malignancy would be an extremely valuable tool for the clinical management of prostatic disease. With recent advances in targeted radiation therapy (2), localization is particularly important for treatment planning.

[*]Address reprint requests to: S.M.N., The Center for Molecular and Functional Imaging, The Department of Radiology and Biomedical Imaging, Box 0946, The University of California, San Francisco, 185 Berry Street, Suite 350, Box 0946, San Francisco, CA 94107. sue@radiology.ucsf.edu.

MRI and MR spectroscopic imaging (MRSI) have been shown to be useful for detecting and staging prostate cancer and for evaluating treatment response (3–8). Numerous studies, both in vivo and ex vivo have demonstrated significantly higher choline/citrate peak area ratios than normal peripheral zone (4,9). Atrophy such as that which occurs after hormone or radiation therapy has been demonstrated as a loss of metabolites and a potential biomarker of effective therapy (8).

Due to the deep location of the prostate gland within the body, its small size, and its complex anatomy, clinical spectroscopic studies of the prostate are difficult. To obtain the high signal to noise and high spatial resolution necessary for MRSI of the prostate, endorectal coils have been used (3,4,10). However, this small coil placed at one side of the prostate exhibits a very nonuniform reception profile. While relative choline to citrate peak area ratios correct for the reception profile and can be used to assess cancer, this does not provide information about individual metabolite levels throughout the prostate. These individual metabolite levels may vary due to differing amounts of atrophy or degree of cancer or potentially Gleason grade of cancer (5). However, they may vary due to the nonuniform reception profile of the endorectal coil.

The current MRSI acquisition method incorporates a point resolved spatial spectroscopy (PRESS) selection, very selective saturation (VSS) pulses (11), three-dimensional (3D) phase encoding, and an endorectal coil inhomogeneous reception. These result in varying metabolite levels and can adversely affect interpretation of the spectra. The inhomogeneous reception profile of the endorectal coil is the largest of these artifacts. A method to remove or reduce this artifact would improve interpretation, so that variations can be attributed to biology or pathology rather than location relative to the endorectal coil. Additionally, such a method could be useful for facilitating interpretation as spectra from different parts of the prostate would not need to be scaled differently to ensure visualization of the peaks.

The goal of this study was to develop and validate a post-processing correction algorithm to remove the effect of the inhomogeneous reception profile of the endorectal coil on PRESS selected, spatially saturated, 3D MRSI data.

MATERIALS AND METHODS

Phantoms and Subjects

A uniform phantom comprised of 5.9 mM choline, 12.4 mM creatine, and 32.5 mM citrate in solution was scanned and MRSI data analyzed. The subject population was comprised of 18 consecutive subjects selected from our database based on the criteria of no prior prostate cancer therapy and an estimated prostate volume <50 cc (mean = 27.4 ± 11.2 cc). This size criteria was used to decrease the variability in spectral metabolites due to biological variability from extensive benign prostatic hyperplasia (BPH) and to have sufficient cases in which the peripheral zone extended anteriorly within the prostate (i.e., not compressed posteriorly and laterally by central gland BPH), thus emphasizing the effect of the endorectal coil reception profile. Written informed consent was obtained from all subjects following a protocol approved by the Committee on Human Research at this institution. The subjects' mean age was 57 ± 7 years old, ranging from 43 to 71 years old. A total of 16 of the subjects had biopsies positive for prostate cancer, with Gleason Scores ranging from Gleason 2 + 3 to Gleason 4 + 4 with a median Gleason Score of 3 + 3. The remaining two patients had biopsies negative for prostate cancer.

MRI

All images and spectra were acquired using a 3T MR scanner (GE Medical Systems, Milwaukee, WI, USA). The GE pelvic phased array and a balloon-inflated endorectal coil probe (Medrad, Inc, Indianola, PA, USA) were used for reception. For spectroscopy, while data was acquired with both the pelvic phased array and the endorectal coil, only the data from the endorectal coil was used due to its much higher signal to noise ratio. Sagittal and axial T1-weighted images were acquired (TR/TE = 600/12). Fast spin echo (FSE) T2-weighted images were acquired in an oblique axial plane with FOV = 14 cm to 16 cm, matrix = 256 × 256, and TR/TE = 5000/108.

The MRSI data was localized to the prostate using PRESS-based selection based upon these images, with x, y, and z dimensions set at 120% of the requested volume to ensure high excitation (greater than ~95%) throughout the desired volume of interest. All data was acquired using a specialized Malcolm Levitt (MLEV)-PRESS MRSI sequence with j-refocusing providing an upright citrate resonance at 3T (12,13) The bandwidths of the RF pulses were 2366.7 Hz for the 90° pulse in the anterior-posterior direction and 6097.5 Hz for the two 180° spectral-spatial pulses (14) in the right-left and superior-inferior directions. VSS pulses (11) were automatically applied to the six edge faces of the desired volume and were graphically applied in up to five additional oblique planes to reduce signal from outside the region of interest and from fat at the corners of the volume. These saturation bands were 30mm wide. MRSI was acquired using 3D phase-encoding with 5.4 × 5.4 × 5.4 mm^3 (0.16 cc) resolution with a TR/TE = 1300 msec/85 msec. 1024 points were acquired over 1000 Hz.

Analyses

MRSI—The MRSI data was filtered with a 3 Hz Gaussian filter, Fourier transformed, baseline corrected, phase and frequency aligned based upon the water peak, and peak areas quantified, using algorithms long established at our institution (15,16). Small variations due to PRESS selection nonuniformity and due to chemical shift differences among the metabolites were not corrected. Peak areas of water, choline, creatine, and citrate were calculated for all spectral voxels within the selected region with less than 10% saturation from the VSS pulses.

Model of the VSS Pulses—The suppression due to the VSS pulses was modeled using RF Tools, a radio frequency modeling package within Matlab (The MathWorks, Inc., Natick, MA, USA) (17). This led to an approximate 97% suppression throughout the 30 mm wide (full width at half maximum [FWHM]) saturation band. The transition from 97% saturation to 3% saturated spanned 1.6 mm. A map was made of the suppression profile by automatically shifting and rotating these bands to their prescribed locations and multiplicatively combining them.

Model of the Endorectal Coil Reception Profile—The reception profile of the endorectal coil was theoretically modeled as described earlier (18). The coil was modeled as a series of 12 straight wire segments, outlining the elliptical shape of the coil, using a major diameter of 87 mm along the main magnetic field axis and a minor diameter of 41.2 mm along the axis across the bore. The Biot Savart law was used to determine the magnetic fields produced by each of these wires in the directions perpendicular to the static magnetic field. A resultant reception profile map was created from the combination of these fields.

Reception profiles maps were also generated for the following rotations around the right-left axis of the image: 5, 10, 18.5, and 20 degrees such that the superior portion of the coil tipped anteriorly, as is commonly found in practice, with an average tip of 18.5 degrees reported in the literature (19). The reception profile maps were additionally generated for rotations of 5, 10, 20, and 40 degrees around the superior-inferior axis of the image. Rotation is common about this axis due to the coil being inserted sagittally and then manually rotated to its more

coronal position. If larger tips are found on initial scout imaging, the coil is rotated to a more coronal orientation.

The T2-weighted images were used to determine the location and rotation of the endorectal coil. The balloon has protrusions which result in semicircle indentations in the rectal wall near the location of the coil. Cursor cross-hairs are placed an indentation diameter away from these two locations on a mid-gland axial image (Fig. 1a). On the sagittal image (Fig. 1b), the coil location is determined based the low signal ‘‘streaks’’ that curve anteriorly and outward from the coil both superiorly and inferiorly. These low signal regions are due to the fact that there is no MR signal received in the superior-inferior (main field direction) and that these coils are only sensitive to this superior-inferior direction at these locations (Fig. 1b). The reception profile map was then aligned to match the location of the coil in the images, incorporating rotation about the superior-inferior axis, i.e., in the axial plane, if necessary. It was assumed there was no motion between the T2-weighted image and the MRSI acquisition.

Sensitivity of Correction to Differences in Coil Rotation and Translation—The simulated reception profile maps for the coil at different tips out of the coronal plane were compared to the reception profile maps generated by modeling the coil without a tip, then rotating the map into the same orientation. The percent difference between these two maps, once normalized, was calculated for a region representing a very large MRSI region in a representative location. This region was $6.5 \times 4.5 \times 3.5$ cm^3 in size, centered at (Left = 0.3, Anterior = 34.0, Superior = 1.2 mm) while the coil was centered at (0,0,0).

To determine if small differences in rotation of the endorectal coil about the R-L axis need to be modeled, the reception profile maps modeled with a rotation were compared to reception profile maps modeled in the coronal plane which were then rotated to the final position. The maps with modeled rotation were divided by the rotated, modeled maps and the mean and SD of intensities calculated for the same, large MRSI region described above. Errors of 5% or less were deemed acceptable.

To determine if errors in measuring the coil position would contribute significant error to the final corrected MRSI data, the correction of uniform phantom data was compared across shifts in coil position in right-left, anterior-posterior, and superior-inferior of: ± 1 to 10 mm, in 1 mm increments.

MRI Combined Pelvic Phased Array and Endorectal Coil Reception Profile Correction—For correcting the images, a reception profile map was generated for the combined pelvic phased array and the endorectal coil setup. The pelvic phased array coils were modeled as an anterior and a posterior set of two coils. Each set had two overlapping 12.5 cm in length square coils with the distance between the centers equal to 10.6 cm. Maps were generated as the magnitude of the map for each coil. Since the prostate is far from the pelvic phased array, small errors in positioning of these coils were ignored. Therefore, the pelvic phased array map was presumed to have no rotation and to be centered in plane the same as the endorectal probe. Also, the anterior array was presumed to always be at 150 mm anterior to the endorectal coil. The posterior array, on the other hand, was presumed to be 125 mm posterior to the endorectal coil. Obviously, these positions will vary slightly from patient to patient, and could be measured and modified for each, but for ease of analysis, these distances were used and historically have worked well for all but very thin patients. These reception profile maps were aligned to the images and the image intensities were divided by the reception profile map on a pixel by pixel basis to correct the images for the inhomogeneous coil reception profile.

MRSI Endorectal Reception Profile Correction—The reception profile map was multiplied by the VSS pulse profile map. This map was then reduced to the MRSI acquired spectral resolution using a 3D sinc interpolation to model the point spread function of the 3D MRSI acquisition. The spectral data at each location was then divided by this matched resolution reception profile map. This was performed for the uniform phantom data and the patient data.

Statistical Analyses

The mean, SD and cumulative histogram of values were computed for the different metabolites for the phantom and for the MRSI regions on the patients. For the phantom study and in the 18 patients, coefficients of variation, c_v = mean/SD, for integrals of the water, choline, creatine, and citrate peaks were calculated before correction and after correction, along with their corresponding percent improvements: $100 \times (c_{v\ \text{before}} - c_{v\ \text{after}})/c_{v\ \text{before}}$.

The metabolite area distributions were analyzed using a Q-Q plot, comparing their distribution to a normal distribution both before and after correction. The R^2 correlation coefficients of the linear fit of the plots were compared before and after correction as a metric of improved correction using a paired t-test. Analysis was done for: 1) the uniform phantom; and 2) the patients using all the unsaturated voxels.

RESULTS

Simulation Studies

As described in the methods, rotations of the coil were simulated and assessed. The percent differences between: 1) maps modeled with a coil rotation; and 2) maps modeled without a coil rotation but then rotated to the target angle, were calculated for a large MRSI region, after normalization to the mean intensity of the region. These demonstrate that for sagittal plane rotations <20°, the mean percent difference is small, 5% or less. As expected, rotations in the axial plane yield virtually no difference between modeled and rotated after modeling, since both right-left and anterior-posterior components are modeled and received by the coils.

Additionally, the percent differences in the coil reception profiles shifted off-center vs. on center were also calculated for the same large MRSI region. These percent differences were <5% for shifts <7 mm in either right-left, anterior-posterior, or superior-inferior directions.

Phantom Studies

Spectral peak area values for a uniform phantom were compared before and after correction for the endorectal coil reception profile. The c_v values calculated for the phantom scan are shown in Table 1 along with their corresponding percent improvements $100 \times (c_{v\ \text{before}} - c_{v\ \text{after}})/c_{v\ \text{before}}$, For both the acquired and corrected cases, the cumulative distribution of water peak areas was plotted versus the cumulative distribution of a normally distributed population in a Q-Q plot (see Fig. 2). In the acquired case, there is a large mismatch at the ends of the distribution, resulting in a linear regression to a straight line yielding an R^2 of 0.89. In the corrected case, the data is close to matching a straight line, with a linear regression correlation coefficient, $R^2 = 0.99$, as shown in Fig. 2, demonstrating near normal distribution of the data.

To demonstrate the impact of the VSS pulses, an image of a phantom with VSS pulses applied is shown in Fig. 3. This image shows the virtually complete suppression of the signals within the bands.

Patient Studies

Representative images and spectra from a prostate cancer patient are shown in Fig. 4. In the acquired case, the image intensity and spectral intensities are high close to the endorectal coil and lower with distance from the endorectal coil. In the corrected case, the image and citrate intensities are more uniform. The metabolites vary by location, with the peripheral zone and the central gland having quite different patterns, but are more uniform throughout the peripheral zone. A region of cancerous peripheral zone is apparent, with greatly decreased citrate. Correcting for the coil reception gives more confidence that a decrease of citrate is due to pathophysiology rather than reception profile.

Figure 5 shows the Q-Q plots for the water, choline, creatine, and citrate for voxels with more than 90% maximum excitation both before and after correction from the example patient of Fig. 4. In all cases, the distribution of peak areas is more normally distributed after coil correction than before. This is demonstrated by higher linear fit correlation coefficients, R^2, in the Q-Q plots after correction (average $R^2 = 0.98 \pm 0.007$) than before correction (0.89 ± 0.066).

For the 18 patients, the mean coefficient of variation, c_v, value for the suppressed water resonance prior to correction was 0.95 ± 0.18 which significantly decreased to 0.66 ± 0.11 after correction, $P < 10^{-6}$, paired *t*-test. The mean R^2 value for the Q-Q plot for the suppressed water resonance for the patients increased from an average of 0.91 prior to correction to an average of 0.95 post-correction ($P = 0.0083$, paired *t*-test).

DISCUSSION

This paper described and validated a post-processing correction algorithm to reduce the effect of the inhomogeneous reception profile of the endorectal coil on prostate MRSI data while incorporating the effects of a sinc-shaped point spread function MRSI acquisition and VSS pulse suppression. The plots of spectra demonstrate an increase in uniformity with this correction. The Q-Q plots for both the phantoms and prostate cancer patients demonstrate that the acquired MRSI peak areas are not fully Gaussian in distribution, whereas they are significantly more Gaussian post correction ($R^2 = 0.96$, mean for water distribution for the combination of the phantom and the patients).

Additionally, the simulations shown here demonstrated that this technique is robust, with <5% average error for rotations of up to 20° of the coil out of the coronal plane, more than typically found in practice (19). Furthermore, the coil profile can be generated on a case-by-case basis. For ease of use in practice, a typical rotation is suggested.

This technique is also very robust across shifts in position and/or in determining the coil location, as the average error is <5% for shifts <7 mm. Another study showed small patient shifts between anatomic imaging acquired before and after an MRSI sequence, reporting an average of 2.6 ± 2.4 mm shifts in position (20). Thus, coil reception profile maps are expected to have small error due to patient shifts and coil localization errors.

While the corrected spectral peak areas are not completely uniform, this is to be expected. The small (<5%) variability in RF excitation across the region of interest was not corrected. Additionally, biologic variability is likely another source of variability, as illustrated by the highest R^2 values for the corrected phantom water values, the second highest R^2 for the water in the patients and the lower R^2 for the metabolites, choline, creatine, and citrate in the patients. A remaining source of variability is errors in quantifying the peak areas. This is in part demonstrated by the lower improvement in the coefficient of variation in choline and creatine versus water and citrate in the phantom data of Table 1, as choline and creatine are more difficult

to quantify due to their overlap with each other and with polyamines. While these variabilities exist, the uniformity increased with reception profile correction and the distribution became significantly more Gaussian, indicating the effect of the inhomogeneous reception profile was reduced. The greater improvement in the phantom versus the patients indicates that the biological heterogeneity of the tissue is not normally distributed—mixing cancerous tissues and central gland tissue, with its frequent BPH, with the peripheral zone tissues leads to variability beyond a normal distribution.

In other work, MRSI data has been acquired with surface coils, primarily for the brain (16, 21–27) and prostate (4,28,29). These data also are affected by the inhomogeneous reception profiles. As ratios of metabolites are frequently used, the MRSI data often is left uncorrected for the inhomogeneous reception profile. Some have addressed the surface coil reception profile effect in MRSI data with different approaches than presented in this work. In one method, the water peaks in MRSI data have been used to correct phased array brain MRSI data for the inhomogeneous reception profiles (21,22). In the prostate, however, water intensities are known to vary greatly among tissue types, like glandular versus stromal BPH, and with treatment, so this technique may not be suitable, especially if water is to be measured.

Another method to address the surface coil reception profiles used array spatial sensitivity encoding technique (ASSET) calibration scans. In recent years, brain MRSI data has been acquired at 3T using a multiple coil array (23–27). Spectra from the individual coils have been weighted by ASSET calibration scans to model their reception profiles and have been combined (23–26). This resulted in MRSI data with the effect of the inhomogeneous reception profiles reduced. Such sensitivity profiles of the surface coils have also been used for parallel imaging of MRSI data (27) and to unalias lipids in MRSI data (26). While these methods have worked well in the brain, they are more challenging in the prostate. Producing a map of coil sensitivity using either an additional image, such as the ASSET calibration scans, or using a low pass filtered version of the actual image or dataset can lead to some image information being ‘‘corrected out’’. This is especially problematic when there are low spatial frequency objects in the image, such as the large, dark rectum next to the prostate. An ASSET calibration scan or a low-pass filtered image of the prostate would retain the rectum, and, when blurred, would lead to a poor representation of the coil sensitivity within the prostate near the rectum. As this is the location of the peripheral zone, where ~70% of the cancers arise, this is problematic for prostate MRSI data. Other features within the prostate (such as hemorrhage or brachytherapy seeds) can also confound this method.

Similar to the current study, theoretical models of the inhomogeneous reception profile of surface coils and models of the selective excitation and the MRSI point spread function have been reported, but only in a limited number of studies (16,30). These models have been used to investigate brain tumor MRSI data (16) and to investigate differences between normal brain gray and white matter (30).

Correcting MRSI data for the inhomogeneous reception profile of surface coils is desirable, due to increased uniformity of peaks in biologically homogeneous tissues, due to resultant likelihood of increased detection of abnormalities and due to ease of presentation of the data, as the same intensity scale can be used and would allow adequate viewing of the full range of spectra. The latter is particularly important when arrays of MRSI are stored as static images, as in many electronic imaging databases.

While choline plus creatine levels can be compared to citrate levels on a voxel by voxel basis, eliminating the need to correct for the coil profiles, this is problematic when citrate is very low, as often occurs with prostate cancer. Additionally, comparisons of levels of choline and citrate to normal levels cannot be made without such a correction as presented here. Such

normalizations are particularly important when comparing data from different patients or exams.

Results of this study demonstrate the feasibility of quantitatively comparing measured metabolite levels in different regions and, ultimately, through an exam normalization, to quantitatively compare metabolites from different times in the same patient and from different patients. This is particularly important for comparing tumor grades with metabolite levels to potentially differentiate tumor grade based upon choline levels (5).

This technique which incorporates theoretically modeling the reception profile and manually identifying the coil location in images has the advantage of not removing image information from nor adding additional noise to the acquired MRSI data. A disadvantage is that the coil location needs to be identified. In the future, this potentially could be automated. Another disadvantage is that noise will appear higher far from the coil, although the signal to noise ratio remains the same. Future research is needed to investigate if such a post-processing correction of MRSI data can improve the detection accuracy, speed, and/or characterization of prostate cancer.

In conclusion, a procedure for reducing the effect of the inhomogeneous reception profile in endorectal coil acquired 3D MRSI prostate data was demonstrated, illustrating increased homogeneity in MRSI data and a significantly more Gaussian distribution of peak areas. This technique has potential to facilitate interpretation of the MRSI data.

Acknowledgments

We acknowledge Dr. Sarah J. Nelson for valuable discussions.

Contract grant sponsor: American Cancer Society; Contract grant number: MRSG-CCE-05-087-01; Contract grant sponsor: National Institutes of Health (NIH); Contract grant number: CA111291.

References

1. American Cancer Society. Cancer Facts & Figures 2008. Atlanta: American Cancer Society; 2008.
2. Hatano K, Araki H, Sakai M, et al. Current status of intensity-modulated radiation therapy (IMRT). Int J Clin Oncol 2007;12:408–415. [PubMed: 18071859]
3. Hricak H, White S, Vigneron D, et al. Carcinoma of the prostate gland: MR imaging with pelvic phased-array coils versus integrated endorectal--pelvic phased-array coils. Radiology 1994;193:703–709. [PubMed: 7972810]
4. Kurhanewicz J, Vigneron DB, Hricak H, Narayan P, Carroll P, Nelson SJ. Three-dimensional H-1 MR spectroscopic imaging of the in situ human prostate with high (0.24–0.7-cm3) spatial resolution. Radiology 1996;198:795–805. [PubMed: 8628874]
5. Kurhanewicz J, Vigneron DB, Nelson SJ. Three-dimensional magnetic resonance spectroscopic imaging of brain and prostate cancer. Neoplasia 2000;2:166–189. [PubMed: 10933075]
6. Chen M, Hricak H, Kalbhen CL, et al. Hormonal ablation of prostatic cancer: effects on prostate morphology, tumor detection, and staging by endorectal coil MR imaging. AJR Am J Roentgenol 1996;166:1157–1163. [PubMed: 8615261]
7. Kalbhen CL, Hricak H, Shinohara K, et al. Prostate carcinoma: MR imaging findings after cryosurgery. Radiology 1996;198:807–811. [PubMed: 8628875]
8. Coakley FV, Teh HS, Qayyum A, et al. Endorectal MR imaging and MR spectroscopic imaging for locally recurrent prostate cancer after external beam radiation therapy: preliminary experience. Radiology 2004;233:441–448. [PubMed: 15375223]
9. Schiebler ML, Miyamoto KK, White M, Maygarden SJ, Mohler JL. In vitro high resolution 1H-spectroscopy of the human prostate: benign prostatic hyperplasia, normal peripheral zone and adeno-carcinoma. Magn Reson Med 1993;29:285–291. [PubMed: 7680746]

10. Schnall MD, Lenkinski RE, Pollack HM, Imai Y, Kressel HY. Prostate: MR imaging with an endorectal surface coil. Radiology 1989;172:570–574. [PubMed: 2748842]
11. Tran TK, Vigneron DB, Sailasuta N, et al. Very selective suppression pulses for clinical MRSI studies of brain and prostate cancer. Magn Reson Med 2000;43:23–33. [PubMed: 10642728]
12. Cunningham CH, Vigneron DB, Marjanska M, et al. Sequence design for magnetic resonance spectroscopic imaging of prostate cancer at 3 T. Magn Reson Med 2005;53:1033–1039. [PubMed: 15844147]
13. Chen AP, Cunningham CH, Kurhanewicz J, et al. High-resolution 3D MR spectroscopic imaging of the prostate at 3 T with the MLEV-PRESS sequence. Magn Reson Imaging 2006;24:825–832. [PubMed: 16916699]
14. Star-Lack J, Vigneron DB, Pauly J, Kurhanewicz J, Nelson SJ. Improved solvent suppression and increased spatial excitation bandwidths for three-dimensional PRESS CSI using phase-compensating spectral/spatial spin-echo pulses. J Magn Reson Imaging 1997;7:745–757. [PubMed: 9243397]
15. Nelson S, Brown T. A new method for automatic quantifcation of 1-D spectra with low signal to noise ratio. J Magn Reson Imaging 1987;84:95–109.
16. Nelson SJ. Analysis of volume MRI and MR spectroscopic imaging data for the evaluation of patients with brain tumors. Magn Reson Med 2001;46:228–239. [PubMed: 11477625]
17. Pauly J, Le Roux P, Nishimura D, Macovski A. Parameter relations for the Shinnar-Le Roux selective excitation pulse design algorithm [NMR imaging]. IEEE Trans Med Imaging 1991;10:53–65. [PubMed: 18222800]
18. Moyher SE, Vigneron DB, Nelson SJ. Surface coil MR imaging of the human brain with an analytical reception profile correction. J Magn Reson Imaging 1995;5:139–144. [PubMed: 7766974]
19. Kim Y, Noworolski SM, Pouliot J, Hsu IJ, Vigneron DB, Kurhanewicz J. Expandable and rigid endorectal coils for prostate MRI: impact on prostate distortion and rigid image registration. Med Phys 2005;32:3569–3578. [PubMed: 16475755]
20. Noworolski SM, Henry RG, Vigneron DB, Kurhanewicz J. Dynamic contrast-enhanced MRI in normal and abnormal prostate tissues as defined by biopsy, MRI and 3D MRSI. Magn Reson Med 2005;53:249–255. [PubMed: 15678552]
21. Wald LL, Moyher SE, Day MR, Nelson SJ, Vigneron DB. Proton spectroscopic imaging of the human brain using phased array detectors. Magn Reson Med 1995;34:440–445. [PubMed: 7500884]
22. Gu M, Kim DH, Mayer D, Sullivan EV, Pfefferbaum A, Spielman DM. Reproducibility study of whole-brain 1H spectroscopic imaging with automated quantification. Magn Reson Med 2008;60:542–547. [PubMed: 18727040]
23. Li Y, Osorio JA, Ozturk-Isik E, et al. Considerations in applying 3D PRESS H-1 brain MRSI with an eight-channel phased-array coil at 3 T. Magn Reson Imaging 2006;24:1295–1302. [PubMed: 17145400]
24. Osorio JA, Ozturk-Isik E, Xu D, et al. 3D 1H MRSI of brain tumors at 3.0 Tesla using an eight-channel phased-array head coil. J Magn Reson Imaging 2007;26:23–30. [PubMed: 17659562]
25. Xu D, Chen AP, Cunningham C, Osorio JA, Nelson SJ, Vigneron DB. Spectroscopic imaging of the brain with phased-array coils at 3.0 T. Magn Reson Imaging 2006;24:69–74. [PubMed: 16410180]
26. Ozturk-Isik E, Crane JC, Cha S, Chang SM, Berger MS, Nelson SJ. Unaliasing lipid contamination for MR spectroscopic imaging of gliomas at 3T using sensitivity encoding (SENSE). Magn Reson Med 2006;55:1164–1169. [PubMed: 16596629]
27. Lin FH, Tsai SY, Otazo R, et al. Sensitivity-encoded (SENSE) proton echo-planar spectroscopic imaging (PEPSI) in the human brain. Magn Reson Med 2007;57:249–57. [PubMed: 17260356]
28. Casciani E, Polettini E, Bertini L, et al. Prostate cancer: evaluation with endorectal MR imaging and three-dimensional proton MR spectroscopic imaging. Radiol Med (Torino) 2004;108:530–541. [PubMed: 15722999]
29. Futterer JJ, Scheenen TW, Huisman HJ, et al. Initial experience of 3 tesla endorectal coil magnetic resonance imaging and 1H-spectroscopic imaging of the prostate. Invest Radiol 2004;39:671–680. [PubMed: 15486528]
30. Noworolski SM, Nelson SJ, Henry RG, et al. High spatial resolution 1H-MRSI and segmented MRI of cortical gray matter and subcortical white matter in three regions of the human brain. Magn Reson Med 1999;41:21–29. [PubMed: 10025607]

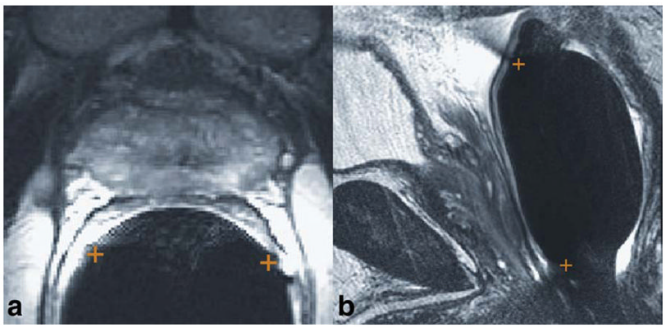

Figure 1.
Identification of the coil location and rotation on (**a**) axial and (**b**) sagittal T2-weighted images. The two ends of the coil are marked with +'s. On the axial image, the locations are identified by the indentations in the rectal wall. On the sagittal image, the locations are identified by the dark streaks that emanate anteriorly and outward from the rectal wall at the superior and inferior ends of the balloon-inflated probe. [Color figure can be viewed in the online issue, which is available at wileyonlinelibrary.com.]

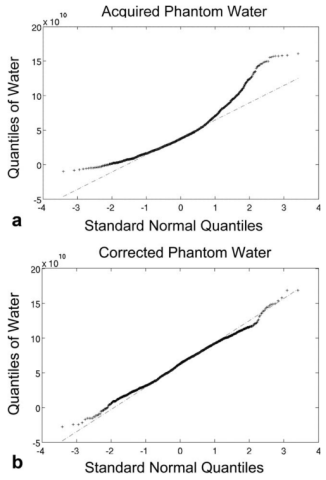

Figure 2.

Assessment of coil correction of water peak areas from a uniform phantom using Q-Q plots of the distribution of the phantom water peak areas as compared to a normal distribution. Data is from the voxels having more than 90% of maximum excitation (within the PRESS selected region and not under the VSS sat bands). **a:** Before correction. **b:** After correction. There is clearly variability in the acquired data that is not all normal in distribution. Once corrected, the MRSI data is more uniform, with the non-normal effects mostly eliminated, as demonstrated by the Q-Q plot better linear fit of the data to a normal distribution (R^2 = 0.99 vs. 0.89).

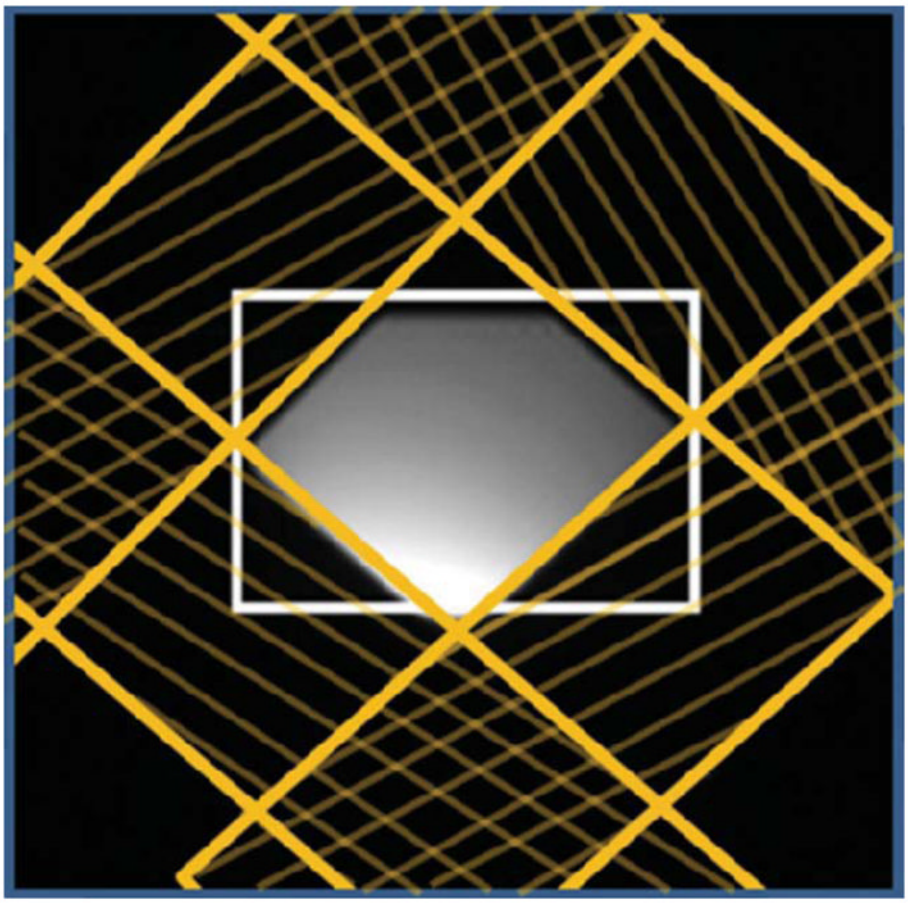

Figure 3.
Image of a phantom with the VSS pulses demonstrating virtually complete suppression of signals within the VSS pulse bands (yellow hashed areas). The white box demarcates the PRESS selected region.

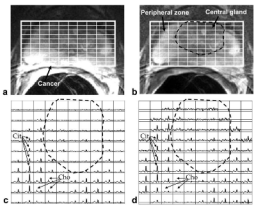

Figure 4.

Example MRI and MRSI from a patient, demonstrating the increased uniformity with coil correction. **a:** Acquired axial MRI. **b:** Corrected MRI from (a). **c:** Acquired MRSI, with spectra from grid locations marked in (a). **d:** Coil corrected MRSI from (c). Cit = citrate, Cho = choline. The citrate peaks decrease anteriorly when acquired (in c) and are more uniform once corrected (in d). In addition to the artifacts due to the coil reception, the MRSI demonstrates biological heterogeneity among healthy peripheral zone tissue (outer, bright tissue), central gland tissue (central, primarily darker tissue, within dashed line) and peripheral zone cancer. The cancer is observable as decreased MRI intensity, clear choline, and markedly decreased citrate (area of spectra with labeled choline and some adjacent voxels).

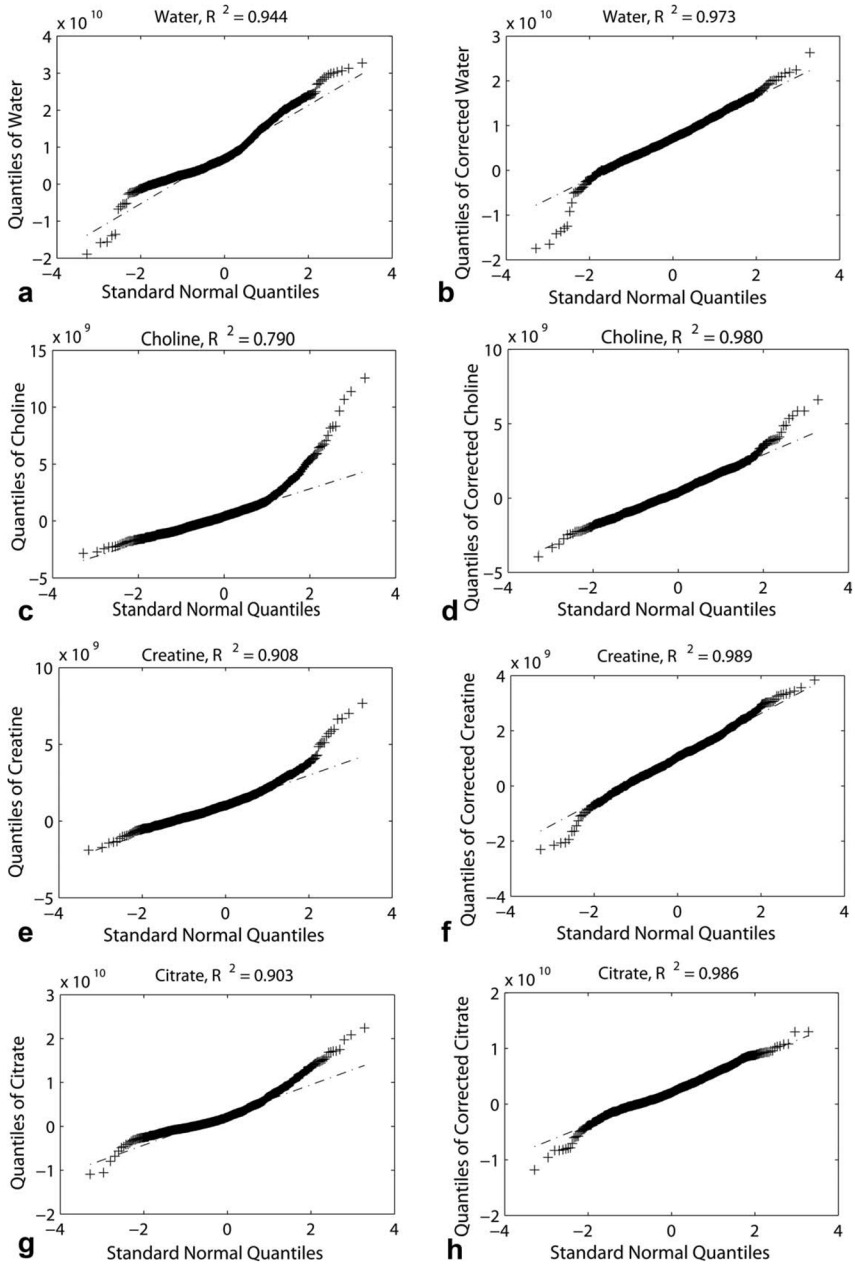

Figure 5.

Q-Q plots of water (**a**, **b**), choline (**c**, **d**), creatine (**e**, **f**), and citrate (**g**, **h**) before (a, c, e, g) and after (b, d, f, h) coil correction for the example subject in Fig. 4. All MRS measures become more normally distributed with coil correction.

Table 1

Coefficient of Variation (c_v) of MRSI Peak Area Values in a Uniform Phantom Before and After Coil Correction, Demonstrating Improved Homogeneity (1430 voxels used)

Peak	c_v Before	c_v After	Improvement (%)
Water	0.77	0.41	46
Choline	0.79	0.58	27
Creatine	0.91	0.76	16
Citrate	0.70	0.40	43